Mondor Hospital, Assistance Publique — Hôpitaux de Paris (AP-HP), Créteil, France; [2]Genetic Department, Cochin Hospital, DMU BioPhyGen, Assistance Publique — Hôpitaux de Paris (AP-HP), Centre-Université Paris Cité, Paris, France; [3]Institut Cochin, Inserm U1016, CNRS UMR8104, UFR de Pharmacie de Paris, Université Paris Cité, CARPEM, Paris, France; [4]Centre of Clinical Investigation, Inserm, Montpellier University Hospital, Montpellier, France; [5]Centre for Epidemiology and Population Health, Inserm, Paris-Saclay University (UVSQ), Villejuif, France; [6]Service de nutrition et gastroentérologie pédiatriques, Hôpital Trousseau, Assistance Publique — Hôpitaux de Paris (AP-HP), Sorbonne Université, Paris, France; [7]INSERM, Centre d'Investigation Clinique 1430, National Referral Center for Neurofibromatoses, Henri-Mondor Hospital, Assistance Publique-Hôpitaux Paris (AP-HP), Créteil, France; [8]Université Paris-Est Créteil (UPEC), Créteil, France; and [9]INSERM U955, IMRB, Créteil, France

[10]These authors contributed equally to this work.

[*]Corresponding author e-mail: laura.fertitta@aphp.fr

SUPPLEMENTARY MATERIAL

Supplementary material is linked to the online version of the paper at www.jidonline.org, and at https://doi.org/10.1016/j.jid.2025.04.026.

REFERENCES

Basto DL, de Souza Vieira G, Andrade-Losso RM, Almeida PN, Riccardi VM, Rozza-de-Menezes RE, et al. Head circumference and anthropometric changes and their relation to plexiform and skin neurofibromas in sporadic and familial neurofibromatosis 1 Brazilian adults: a cross-sectional study. Orphanet J Rare Dis 2022;17:341.

Bergqvist C, Servy A, Valeyrie-Allanore L, Ferkal S, Combemale P, Wolkenstein P, et al. Neurofibromatosis 1 French national guidelines based on an extensive literature review since 1966. Orphanet J Rare Dis 2020;15:37.

Blundell J, Dulloo A, Salvador J, Frühbeck G, EASO SAB. Working Group on BMI. Beyond BMI–phenotyping the obesities. Obes. Facts 2014;7:322–8.

Da Silva FM, Jorge AA, Malaquias A, Da Costa Pereira A, Yamamoto GL, Kim CA, et al. Nutritional aspects of Noonan syndrome and Noonan-related disorders. Am J Med Genet A 2016;170:1525–31.

De Souza M, Jansen A, Martins A, Rodrigues L, De Rezende N. Nutrient intake in neurofibromatosis type 1: a cross-sectional study. Nutrition 2015;31:858–62.

Ferrara U, Tortora C, Rosano C, Assunto A, Rossi A, Pagano S, et al. Bone metabolism in patients with type 1 neurofibromatosis: key role of sun exposure and physical activity. Sci Rep 2022;12:4368.

Fontbonne A, Currie A, Tounian P, Picot MC, Foulatier O, Nedelcu M, et al. Prevalence of overweight and obesity in France: the 2020 Obepi-Roche study by the "Ligue Contre l'Obésité". J Clin Med 2023;12:925.

Johansson E, Kallionpää R, Böckerman P, Peltonen S, Peltonen J. The rare disease neurofibromatosis 1 as a source of hereditary economic inequality: evidence from Finland. Genet Med 2022;24:870–9.

Kallionpää RA, Uusitalo E, Leppävirta J, Pöyhönen M, Peltonen S, Peltonen J. Prevalence of neurofibromatosis type 1 in the Finnish population. Genet Med 2018;20:1082–6.

Martins AS, Jansen AK, Rodrigues LOC, Matos CM, Souza MLR, Miranda DM, et al. Increased insulin sensitivity in individuals with neurofibromatosis type 1. Arch Endocrinol Metab 2018;62:41–6.

Petruzzelli M, Wagner EF. Mechanisms of metabolic dysfunction in cancer-associated cachexia. Genes Dev 2016;30:489–501.

Souza MLR, Jansen AK, Rodrigues LOC, Vilela DLS, Kakehasi AM, Martins AS, et al. Increased resting metabolism in neurofibromatosis type 1. Clin Nutr ESPEN 2019;32:44–9.

Stevenson D, Moyer-Mileur L, Carey J, Quick J, Hoff C, Viskochil D. Case-control study of the muscular compartments and osseous strength in neurofibromatosis type 1 using peripheral quantitative computed tomography. J Musculoskelet Neuronal Interact 2005;5:145–9.

Summers M, Vasiljevski E, Mikulec K, Peacock L, Little D, Schindeler A. Developmental dosing with a MEK inhibitor (PD0325901) rescues myopathic features of the muscle-specific but not limb-specific Nf1 knockout mouse. Mol Genet Metab 2018;123:518–25.

Wen X, Zhang B, Wu B, Xiao H, Li Z, Li R, et al. Signaling pathways in obesity: mechanisms and therapeutic interventions [published correction appears in Signal Transduct Target Ther 2022;7:369]. Signal Transduct Target Ther 2022;7:298.

ANTXR2 Deficiency Promotes Cellular Senescence and Chondroid Differentiation in Hyaline Fibromatosis Syndrome Fibroblasts

JID Open

Journal of Investigative Dermatology (2025) **145,** 2911–2916; doi:10.1016/j.jid.2025.04.022

TO THE EDITOR

Hyaline fibromatosis syndrome (HFS) is a rare autosomal recessive disorder caused by biallelic loss-of-function variants in *ANTXR2*. HFS encompasses 2 variants: (i) juvenile hyaline fibromatosis, with milder symptoms, and (ii) infantile systemic hyalinosis, associated with severe systemic involvement and early morbidity and characterized by hyaline fibrous tissue accumulation in skin and organs, with subcutaneous nodules present in over 80% of patients (Shieh et al, 2008). ANTXR2 is a type I transmembrane protein, mostly studied for its role as the major receptor for the anthrax toxin (Liu et al, 2009). It has been proposed that ANTXR2 maintains extracellular matrix (ECM) homeostasis by binding to collagen VI and regulating its endocytosis and intracellular degradation (Bürgi et al, 2017). However, we previously failed to confirm a role for ANTXR2 as a collagen VI receptor (Przyklenk et al, 2022). Moreover, a loss of collagen VI binding fails to explain the diverse clinical features of HFS, including nodule localization, cellular morphology, and unique collagen characteristics such as "zebra collagen" (Breier et al, 1997; Deuquet et al, 2012; Kitano et al, 1972). Mutations in the cognate receptor ANTXR1 cause GAPO (growth retardation, alopecia, pseudoanodontia and optic

Abbreviations: ECM, extracellular matrix; HFS, hyaline fibromatosis syndrome; MMP, matrix metalloproteinase

Accepted manuscript published online 12 May 2025; corrected proof published online 6 June 2025

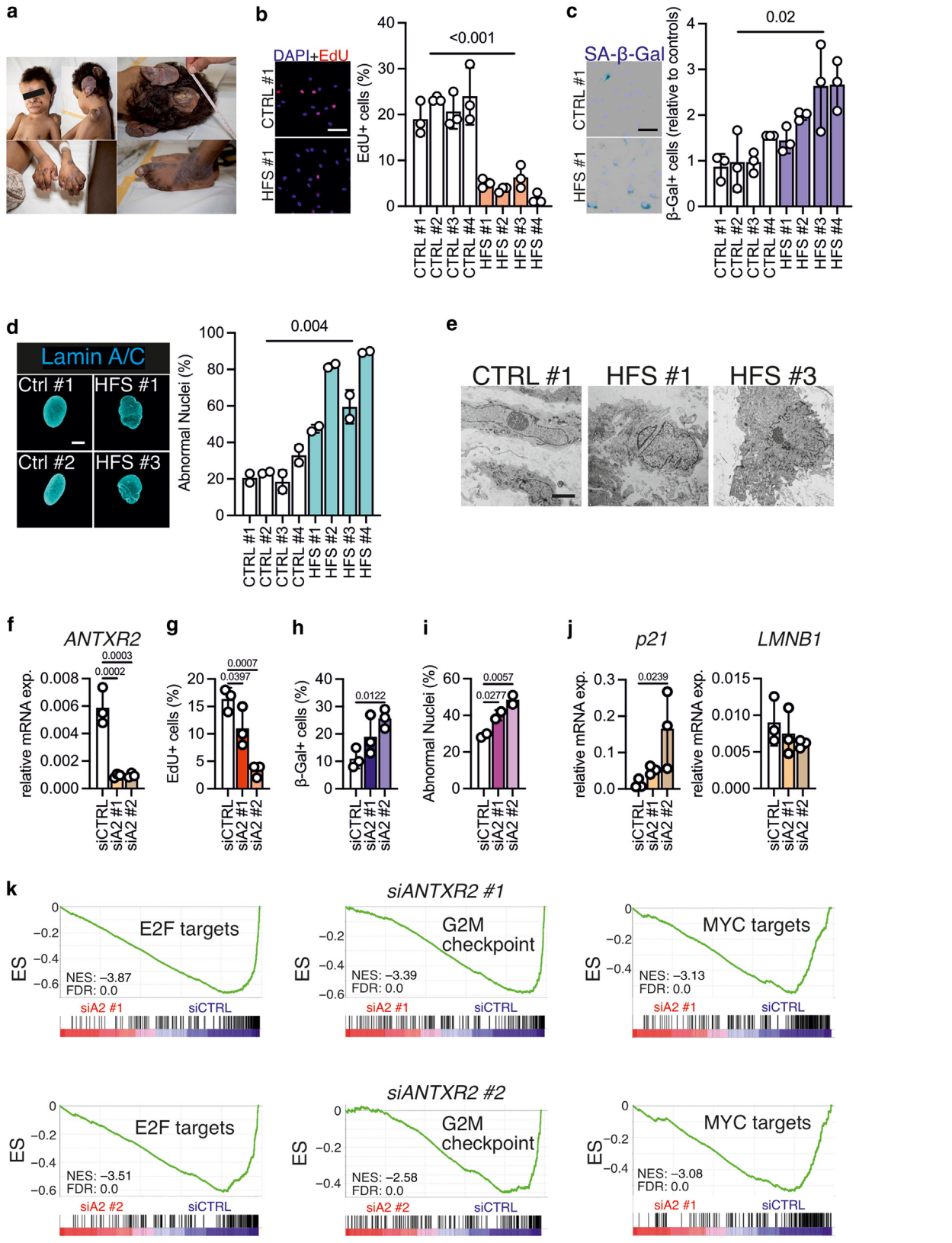

Figure 1. HFS and ANTXR2-depleted fibroblasts exhibit features of cellular senescence. (**a**) Clinical phenotypes of the index patient from family 3 (HFS #3). Written informed consent was obtained for publication of the image. (**b**) Representative images and quantification of EdU incorporation in control and HFS fibroblasts. n = 3 independent experiments, >500 cells per sample. Bar = 100 μm. (**c**) Representative images and quantification of SA-β-Gal expression in control and HFS fibroblasts. n = 3 independent experiments; 100 cells per sample were quantified for each cell line. Bar = 100 μm. (**d**) Representative lamin A/C immunostaining of the indicated cell lines showing nuclear defects in HFS fibroblasts. The bar chart on the right shows the frequency of abnormal nuclei in the different fibroblast lines. n = 3 independent experiments, 100 cells sample. Bar = 10 μm. In the graphs in **b**, **c**, and **d**, *P*-values were calculated using an unpaired *t*-test by pooling all individual control and HFS samples. (**e**) Transmission electron micrograph of the indicated control and HFS fibroblasts.

atrophy) syndrome. We have recently shown that ANTXR1 deficiency promotes fibroblast senescence, suggesting that GAPO syndrome may therefore be reconsidered as a progeroid disorder (Przyklenk et al, 2024).

To test whether ANTXR2 loss of function may have similar consequences, we analyzed primary dermal fibroblasts from nonlesional skin of 4 patients with HFS with 3 different *ANTXR2* allelic variants, including 1 that, to our knowledge, has not previously been reported (HFS #3 and #4) (Figure 1a, Supplementary Figure S1a and b, and Supplementary Tables S1 and S2), and compared them with those from age-matched healthy donors. HFS fibroblasts exhibited abnormal morphology, slower growth, and reduced 5-ethynyl-2′-deoxyuridine incorporation, indicating impaired proliferation (Figure 1b and Supplementary Figure S1c). These cells also showed elevated senescence-associated-β-galactosidase activity, higher *p21*, and reduced *LMNB1* mRNA levels, consistent with cellular senescence (Figure 1c and Supplementary Figure S1d). Nuclear morphology abnormalities were prevalent in HFS fibroblasts, as evident also by transmission electron microscopy (Figure 1d and e and Supplementary Figure S1e). Interestingly, plating HFS fibroblasts on collagen I or fibronectin improved nuclear morphology, suggesting that ECM−actin dynamics influence nuclear envelope integrity. However, cell spreading on ECM substrates was similar between HFS and control fibroblasts (Supplementary Figure S1f and g). ANTXR2 knockdown in normal primary dermal fibroblasts induced comparable proliferation defects and increased senescence markers and nuclear abnormalities (Figure 1f–j). Transcriptomic analysis showed downregulation of proliferation-related gene signatures (Figure 1k). Senescent fibroblasts alter ECM composition, a hallmark also observed in HFS, which features connective tissue disruption due to hyaline material accumulation (Figure 1a). Despite the reduced growth rate of HFS fibroblasts, we were able to analyze the secretome of HFS #1 fibroblasts using an unbiased mass spectrometry approach. Comparing it with 2 controls (CTRL #1 and #2), we identified 75 significantly dysregulated matrisome proteins (Supplementary Figure S2a and b). Downregulated proteins included the core ECM components collagens and fibrillin−microfibril network glycoproteins, such as LTBP1, whereas prominent upregulated ones, such as aggrecan and vitrin, are typically cartilage specific (Figure 2a). These changes were supported by transcriptome analysis, revealing gene expression contributing to ECM dysregulation (Supplementary Figure S2c–f). RT-qPCR and immunofluorescence microscopy confirmed aggrecan deposition and reduced LTBP1 levels in HFS (Figure 2b and c). Importantly, beyond quantitative differences, we observed profound qualitative alterations of ECM organization in cultures of HFS fibroblasts. Patient fibroblasts deposited ECM in a disorganized manner, forming irregular, dense fibril clusters regardless of the ECM component tested (Figure 2d and Supplementary Figure S3). This is in sharp contrast to the organized fibrils seen in controls. Transmission electron microscopy of cell layers confirmed patchy ECM with disorganized material, lacking the distinct fibrillar architecture observed in controls (Figure 2e). Although the 3 major collagen VI chains did not display quantitative differences at protein and transcript levels, collagen VI organization was markedly disrupted, as revealed by ultrastructural analysis coupled with immunogold labeling (Figure 2f–h), supporting altered collagen biosynthesis. These findings indicate a broad disruption of ECM structure and assembly in cultures of HFS fibroblasts, extending beyond gene expression changes. Senescent fibroblasts commonly exhibit altered extracellular protease activity. Secretome interrogation showed similar basal levels of matrix metalloproteinases (MMPs) in HFS #1 fibroblasts (Supplementary Figure S4a). Nevertheless, gelatin zymography revealed impaired MMP induction in HFS #1 culture media after TNF-α treatment with ∼3- and ∼10-fold lower induction of *MMP2* and *MMP9* mRNA, respectively. In HFS #3 and #4 fibroblasts, both MMP2 and pro-MMP9 stimulation by TNF-α was completely blunted. MMP14, essential for pro-MMP2 activation, showed comparable levels in HFS and control cultures, as did collagen VI (Supplementary Figure S4b and c). A collagen dissolution assay demonstrated that HFS fibroblasts were less active under both basal and TNFα-stimulated conditions (Figure 2l). Furthermore, TNFα treatment did not alter ECM deposition in HFS and control fibroblasts, suggesting that MMP dysregulation alone is likely not directly responsible for the aberrant ECM deposition observed in HFS cultures (Supplementary Figure S5). Transient ANTXR2 depletion in fibroblasts did not cause a defect in MMP activation or collagen VI α1 accumulation similar to that in HFS fibroblasts (Figure 2m), indicating that MMP alterations are not a direct consequence of ANTXR2 deficiency. Similarly, transient knockdown did not induce visible changes in ECM architecture or trigger a chondrogenic secretome switch but led to the increased release of several collagens into the medium (Supplementary Figure S6). This confirms that the phenotypic switch

Bar = 2 μm. (**f**) Expression levels of *ANTXR2* in fibroblasts transfected with the indicated siRNAs as assessed by RT-qPCR. n = 3 independent experiments. (**g**) Reduced proliferation in CTRL #2 fibroblasts transfected with ANTXR2-specific siRNAs as assessed by EdU incorporation rates. n = 3 independent experiments (>500 cells each). (**h**) Increased SA-β-Gal expression in ANTXR2-silenced fibroblasts. n = 3 independent experiments, 100 cells each. (**i**) Increased fraction of misshapen nuclei in fibroblasts transfected with *ANTXR2*-specific siRNAs as assessed by LMNA/C staining. n = 2 independent experiments (100 cells each). (**j**) RT-qPCR analysis for *p21* and *LMNB1* expression in fibroblasts transfected with the indicated siRNAs. n = 3 independent experiments. (**k**) Plots of the running enrichment scores for gene sets related to cell proliferation (E2F targets, G2M checkpoint, and MYC targets) as the analysis walks down the ranked gene lists generated by transcriptome analysis of primary fibroblasts transfected with 2 *ANTXR2*-specific siRNAs or a control siRNA. n = 3. In all the bar graphs in this figure, each data point represents an independent experiment. EdU, 5-ethynyl-2′-deoxyuridine; ES, enrichment score; FDR, false discovery rate; HFS, hyaline fibromatosis syndrome; NES, normalized enrichment score; SA-β-Gal, senescence-associated-β-galactosidase; siCTRL, control-targeted small interfering RNA; siRNA, small interfering RNA.

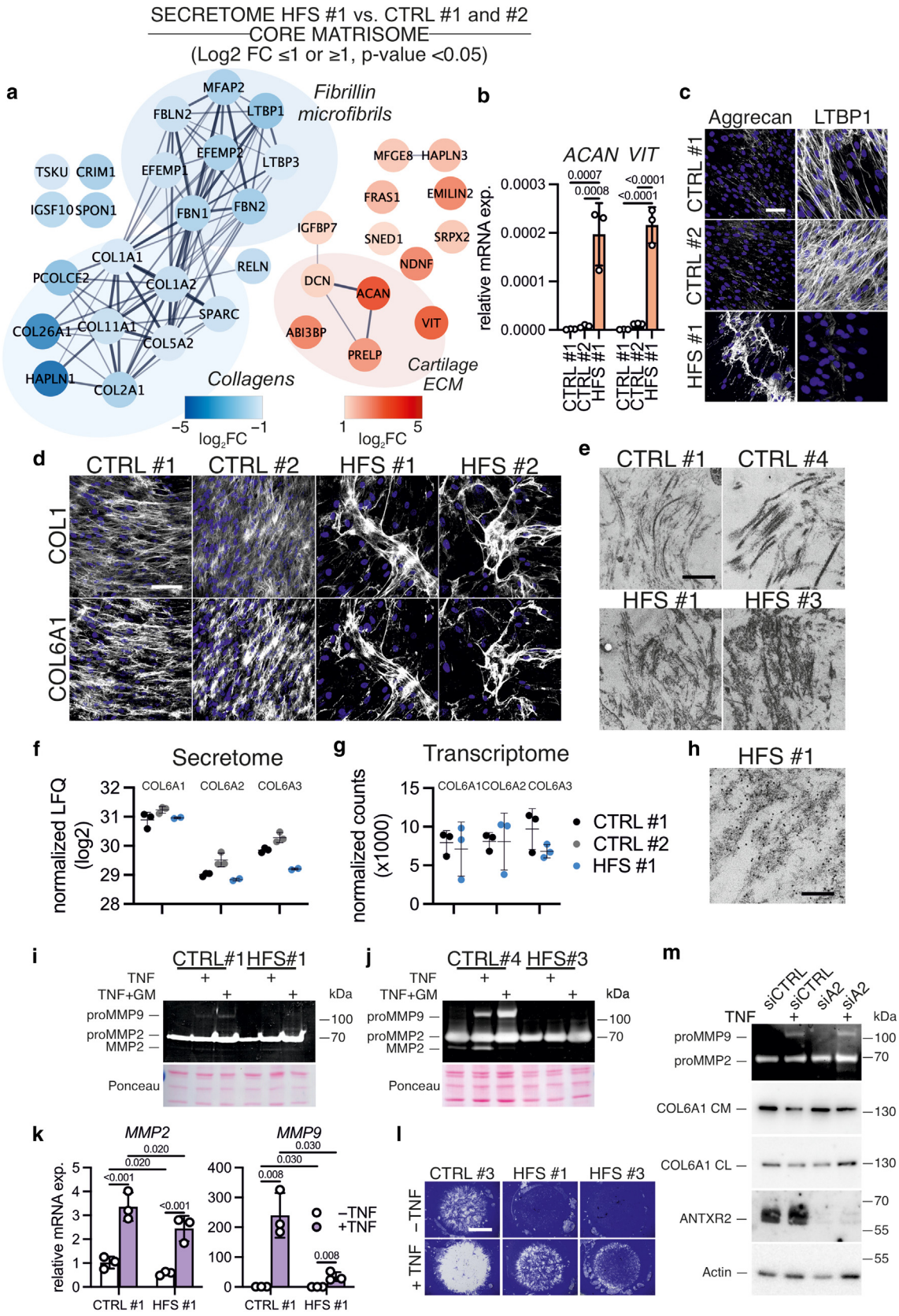

Figure 2. Disrupted ECM organization and MMP activity in HFS fibroblasts (**a**) String network of core matrisome components that were found to be significantly less or more abundant in the secretome analysis of HFS fibroblasts. The color of the nodes (blue for reduced and red for increased proteins) reflects the $\log_2$ fold change of HFS #1 versus CTRL #1 fibroblasts. (**b**) RT-qPCR validation of the upregulation at the mRNA level of 2 matrisome components, aggrecan and vitrin, that are normally expressed only in cartilage. n = 3, with 1-way ANOVA. (**c**) Immunofluorescence staining of confluent fibroblast monolayers labeled with antibodies against aggrecan and LTBP1. Bar = 100 μm. (**d**) Representative confocal images of the indicated fibroblasts lines double stained with antibodies

observed in HFS fibroblasts probably results from a long-term, chronic—or possibly developmental—absence of the receptor.

In summary, we demonstrate that ANTXR2 deficiency in fibroblasts is linked to a complex phenotype involving cellular senescence, abnormal ECM biosynthesis with a chondroid-like secretome, and impaired MMP activation. These features align with HFS clinical manifestations: chondroid histological appearance of the subcutaneous nodules and their preferential localization in skin areas covering articular joints. Expression of aggrecan, a major proteoglycan of hyaline cartilage, previously reported in Hutchinson-Gilford progeria (Lemire et al, 2006), may contribute to the originally described "hyaline" appearance of the amorphous material of HFS nodules. Aggrecan forms complexes with collagen VI and protects cartilage collagen from MMP-mediated degradation. It therefore potentially contributes to altered collagen accumulation. Our findings clarify the clinical overlap between HFS and Winchester syndrome (also known as MONA [multicentric osteolysis nodulosis and arthropathy]), linked to *MMP2* mutations. A similar phenotype in *Antxr2*-deficient and *Mmp2*-knockout mice, namely defective parturition and uterine fibrosis, further supports the connection between these proteins (Bürgi et al, 2017; Kalev-Altman et al, 2023).

Our results suggest that a complex interplay between altered ECM and a fibroblast phenotypic switch may drive disease progression. The precise mechanisms through which ANTXR2 regulates ECM composition remain unknown. Beyond its proposed role as a collagen VI receptor, ANTXR2 may act more broadly as a receptor for various ECM molecules, modulate the function of other cell-surface receptors involved in ECM assembly, influence ECM secretion and assembly processes, or affect the activity of proteases critical for ECM remodeling.

Although further studies are needed to test these mechanisms and to better characterize fibroblast alterations and ECM pathology, our findings offer additional insights into HFS and highlight potential therapeutic strategies, such as targeting senescent cells.

ETHICS STATEMENT

This study was performed in accordance with the Declaration of Helsinki. Human primary cell lines included in this study were approved as part of this study protocol. This human study was approved by Pediatric Genetics, Center for Pediatric and Adolescent Medicine, University Hospital Freiburg. All parents, guardians, or next of kin provided written informed consent for the minors to participate in this study.

DATA AVAILABILITY STATEMENT

The RNA-sequencing data generated in this study have been deposited in the Gene Expression Omnibus database under accession code GSE294791 (https://www.ncbi.nlm.nih.gov/geo/query/acc.cgi?acc=GSE294791). Secretome datasets are available as supplementary information (Supplementary Table S3). Additional data supporting this study's findings are available upon request from the corresponding author.

KEYWORDS

ANTXR2; Fibrosis; Hyaline fibromatosis syndrome; MMPs

ORCIDs

Alvise Schiavinato: http://orcid.org/0000-0002-8969-4074
Rübsam Matthias: http://orcid.org/0000-0002-0012-2601
Zigrino Paola: http://orcid.org/0000-0002-7470-0064
Wagener Raimund: http://orcid.org/0000-0003-3186-017X

CONFLICT OF INTEREST

The authors state no conflict of interest.

ACKNOWLEDGMENTS

We thank patients and families for consenting to the use of data and materials. Special thanks to Thomas Krieg for providing control fibroblasts for small interfering RNA transfection and manuscript feedback. We appreciate Birgit Kobbe's technical assistance and the guidance of Jan-Wilm Lackmann and Stefan Müller from the Cologne Excellence Cluster on Cellular Stress Responses in Aging-Associated Disease Proteomic Facility. We thank Manuel Koch and Gerhard Sengle for collagen XII and fibrillin-1 and -2 antibodies. This research was funded by Deutsche Forschungsgemeinschaft project identification 384170921 (FOR2722/B1-407164210 to MP and RW), PA660/12-2 (MP), SCHI 1627/2-2 (AS), project number 516569227 (ZI1231/3-1 to PZ), by Köln Fortune project number 147/2024 and by the Center for Molecular Medicine Cologne (CMMC), Project-ID C10 to AS. EL is supported by Deutsche Forschungsgemeinschaft (SFB1143, principal investigator) and the European Union (grants 754825 and 847078).

AUTHOR CONTRIBUTIONS

Conceptualization: AS; Funding Acquisition: MP, RW, AS; Investigation: AS, AP-Z, MM, SK, MR, PZ, EL, AW; Writing - Original Draft Preparation: AS; Writing - Review and Editing: AS, MR, PZ, EL, MP, RW

***Alvise Schiavinato*[1,2,3,9,*], *Arthur-Lauri Pasanen-Zentz*[1,9], *Matthias Mörgelin*[4], *Anika Wehrle*[5], *Shreya Karmacharya*[1], *Matthias Rübsam*[6,7], *Paola Zigrino*[8], *Raimund Wagener*[1], *Mats Paulsson*[1,3] *and Ekkehart Lausch*[5]**

[1]Center for Biochemistry, Medical Faculty, University of Cologne, Cologne, Germany; [2]Department of Pediatrics and Adolescent Medicine, Faculty of Medicine, University Hospital Cologne, Cologne, Germany; [3]Center for Molecular Medicine Cologne (CMMC), University of Cologne, Cologne, Germany; [4]Colzyx AB, Lund, Sweden; [5]Pediatric Genetics, Center for Pediatric and Adolescent Medicine, University Hospital Freiburg, Freiburg, Germany; [6]Department Cell Biology of the Skin, University Hospital Cologne, University of Cologne, Cologne, Germany; [7]Cologne Excellence Cluster on Cellular Stress Responses in Aging-Associated Disease (CECAD), University Hospital Cologne, University of Cologne, Cologne, Germany; and [8]Department of Dermatology and Venereology, Faculty of Medicine and University Hospital Cologne, Germany

specific for COL1 and COL6A1. Bar = 100 μm. (**e**) Transmission electron micrographs of the indicated control and HFS fibroblasts. In control fibroblast, the ECM looks regularly organized around the cells. Moreover, banded collagen fibrils (most likely collagen I fibrils) are surrounded by less electron-dense microfibrillar material that comprises bona fide collagen VI microfibrils. On the other hand, HFS fibroblasts produced electron-dense patches of ECM deposits irregularly interspersed between the cells. The structure of these deposits was highly disordered, and it was not possible to identify their different constituents. Bar = 500 nm. Dot plots showing the relative abundance of the 3 major collagen VI chains in the (**f**) secretome and (**g**) transcriptome of the indicated fibroblasts. Each data point is an independent sample. (**h**) Immunogold localization of collagen VI in the ECM produced by HFS fibroblasts. Bar = 250 nm. (**i, j**) Gelatin zymography of supernatants and cell lysates derived from the indicated fibroblast lines. Cells were left untreated (denoted as NT) or treated with 10 ng/ml TNFα alone or with 50 μM of the MMP inhibitor GM6001 for 48 hours before medium collection and analysis. Ponceau staining of lysates was used as a loading control. (**k**) RT-qPCR analysis of *MMP2* and *MMP9* in the indicated fibroblasts left untreated or treated for 48 hours with 10 ng/ml TNFα. Three independent samples for each condition were used, 2-way ANOVA. (**l**) Collagenolytic activity of the indicated fibroblasts seeded on a reconstituted COL1 film in the absence (NT) or presence of TNFα. Bar = 2 mm (**m**) Primary fibroblasts transfected with the indicated siRNA were grown for 2 days in normal medium and then switched to serum free medium for 2 more days. Culture media and cell layers were then collected and analyzed by gelatin zymography and immunoblot with the indicated antibodies. COL1, collagen I; ECM, extracellular matrix; FC, fold change; HFS, hyaline fibromatosis syndrome; MMP, matrix metalloproteinase; siRNA, small interfering RNA.

[9]These authors contributed equally to this work.

[*]Corresponding author e-mail: aschiav1@uni-koeln.de

SUPPLEMENTARY MATERIAL

Supplementary material is linked to the online version of the paper at www.jidonline.org, and at https://doi.org/10.1016/j.jid.2025.04.022.

REFERENCES

Breier F, Fang-Kircher S, Wolff K, Jurecka W. Juvenile hyaline fibromatosis: impaired collagen metabolism in human skin fibroblasts. Arch Dis Child 1997;77:436–40.

Bürgi J, Kunz B, Abrami L, Deuquet J, Piersigilli A, Scholl-Bürgi S, et al. CMG2/ANTXR2 regulates extracellular collagen VI which accumulates in hyaline fibromatosis syndrome. Nat Commun 2017;8:15861.

Deuquet J, Lausch E, Superti-Furga A, van der Goot FG. The dark sides of capillary morphogenesis gene 2. EMBO J 2012;31:3–13.

Kalev-Altman R, Becker G, Levy T, Penn S, Shpigel NY, Monsonego-Ornan E, et al. Mmp2 deficiency leads to defective parturition and high dystocia rates in mice. Int J Mol Sci 2023;24:16822.

Kitano Y, Horiki M, Aoki T, Sagami S. Two cases of juvenile hyalin fibromatosis. Some histological, electron microscopic, and tissue culture observations. Arch Dermatol 1972;106:877–83.

Lemire JM, Patis C, Gordon LB, Sandy JD, Toole BP, Weiss AS. Aggrecan expression is substantially and abnormally upregulated in Hutchinson-Gilford progeria syndrome dermal fibroblasts. Mech Ageing Dev 2006;127:660–9.

Liu S, Crown D, Miller-Randolph S, Moayeri M, Wang H, Hu H, et al. Capillary morphogenesis protein-2 is the major receptor mediating lethality of anthrax toxin in vivo. Proc Natl Acad Sci USA 2009;106:12424–9.

Przyklenk M, Heumüller SE, Freiburg C, Lütke S, Sengle G, Koch M, et al. Lack of evidence for a role of anthrax toxin receptors as surface receptors for collagen VI and for its cleaved-off C5 domain/endotrophin. iScience 2022;25:105116.

Przyklenk M, Karmacharya S, Bonasera D, Pasanen-Zentz AL, Kmoch S, Paulsson M, et al. ANTXR1 deficiency promotes fibroblast senescence: implications for GAPO syndrome as a progeroid disorder. Sci Rep 2024;14:9321.

Shieh JT, Hoyme HE, Arbour LT. Hyaline fibromatosis syndrome. In: Adam MP, Feldman J, Mirzaa GM, Pagon RA, Wallace SE, Amemiya A, editors. GeneReviews® [Internet]. Seattle, WA: University of Washington, Seattle; 2008. XX [Updated 2023 May 11].

Environmental Exposure to Particulate Matter 10 and Mycosis Fungoides: No Evidence of Increased Risk

JID Open

Journal of Investigative Dermatology (2025) **145,** 2916–2919; doi:10.1016/j.jid.2025.03.025

TO THE EDITOR

Mycosis fungoides (MF) is the most common type of cutaneous T-cell lymphoma characterized by the clonal proliferation of skin-homing CD4-positive T cells that tend to colonize the epidermis (Wohl and Tur, 2007).

The increasing incidence of MF has prompted speculation about the role of environmental and lifestyle factors in the risk of lymphoproliferative diseases (Wohl and Tur, 2007). Continuous activation of skin T helper lymphocytes is believed to lead to the malignant transformation of specific clones. Potential risk factors include occupational chemicals exposure, radiation, drugs, and infections. In addition, chronic inflammation and sustained immune activation may select neoplastic clones. These factors may explain, along with exposure to systemic immunosuppressive therapies, the increased risk of cutaneous T-cell lymphoma in patients with psoriasis (Bellinato et al, 2022).

The specific link between environmental particulate air pollution exposure and the risk of MF has been poorly investigated. Recent epidemiologic studies found that patients with cutaneous T-cell lymphoma reside in urban areas near benzene- and trichloroethylene-emitting sites (Korgavkar et al, 2013). However, the role of pollutants in the incidence of cutaneous T-cell lymphoma is not yet clear, because there are clusters with high incidence near areas with low incidence (Korgavkar et al, 2013). The aim of this study was to assess the association between particulate matter (PM) exposure and the risk of MF. This case-control study included histopathologically confirmed MF cases consecutively recorded at the University Hospital of Verona and Bologna (Figure 1). The cases were matched with healthy controls who attended the clinics for nevi monitoring during the same time and from the same geographic area in a 1:10 ratio. To avoid potential biases, the geographic distribution of cases and controls was verified using geographic mapping software. This allowed us to ensure that cases and controls were similarly distributed across the study areas of Verona and Bologna, minimizing the risk of topographical confounding. We excluded patients who had moved to another province at the beginning of the study and omitted from the analysis those who relocated during the follow-up period. Sociodemographic data, including age, sex, current or previous smoking habits, and residential address, were collected for both cases and controls. The residential address was used to determine the average daily exposure to coarse PM (2.5–10.0 μm in diameter, ie, PM10) from January 1, 2013 to January 1, 2021. PM10 mass concentrations at a 1 km^2 spatial resolution and daily temporal resolution were estimated using a space-time statistical model, with the

Abbreviations: CI, confidence interval; HL, Hodgkin lymphoma; MF, mycosis fungoides; PM, particulate matter

Accepted manuscript published online 8 April 2025; corrected proof published online 26 April 2025

SUPPLEMENTARY REFERENCE

Deuquet J, Lausch E, Guex N, Abrami L, Salvi S, Lakkaraju A, et al. Hyaline fibromatosis syndrome inducing mutations in the ectodomain of anthrax toxin receptor 2 can be rescued by proteasome inhibitors. EMBO Mol Med 2011;3: 208–21.

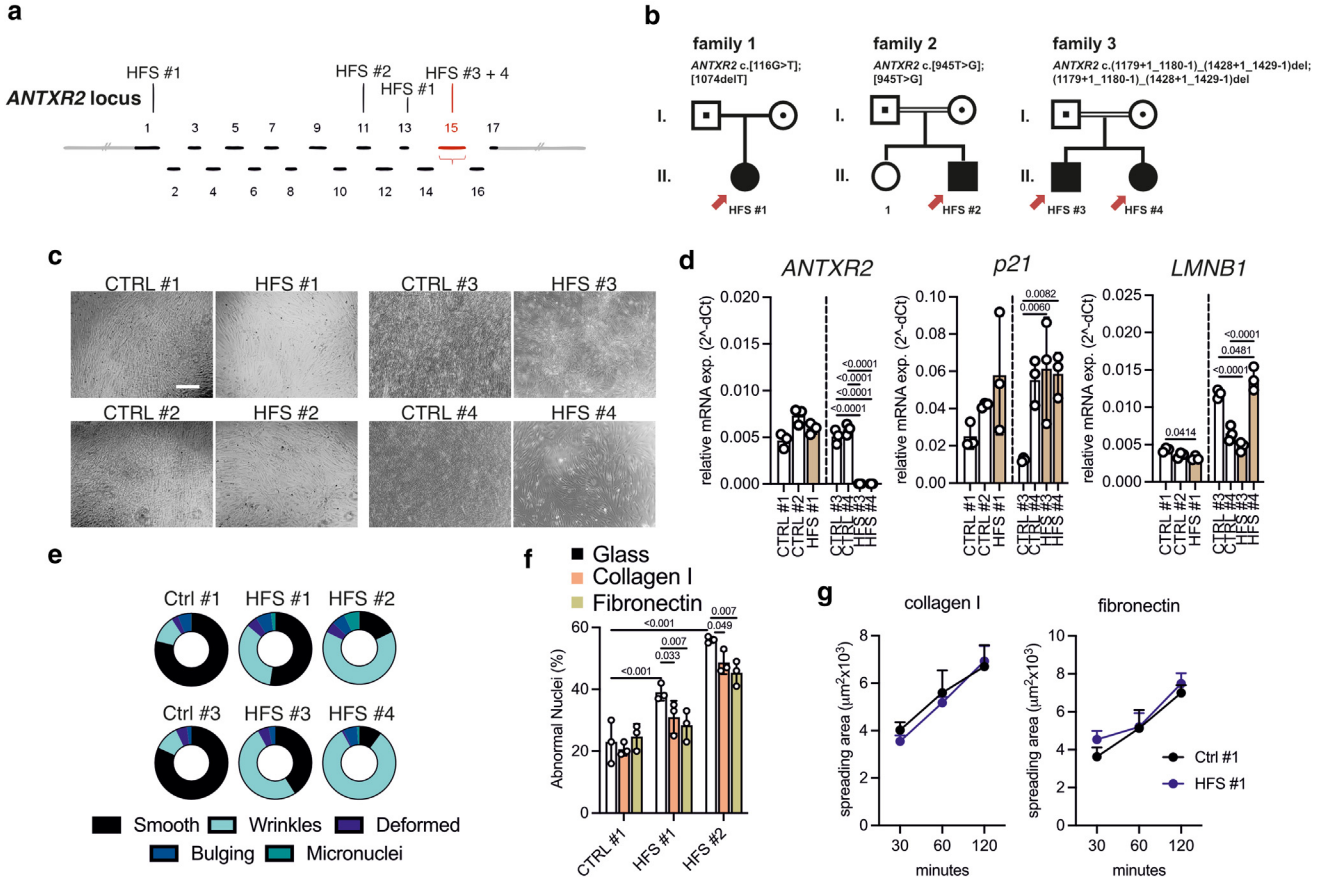

Supplementary Figure S1. Characterization of ANTXR2 allelic variants and cellular phenotypes in HFS patient-derived fibroblasts. (**a**) Schematic representation of the 17-exon *ANTXR2* gene, indicating the localization of pathogenic variants in the 4 patients included in this study. HFS #1 and #2 were described before in (1) as patient 1 and 3, respectively. (**b**) Pedigree analysis of affected individuals from 3 unrelated families carrying *ANTXR2* variants. (**c**) Representative bright-field microscopy images of control and HFS fibroblasts grown for 7 days in the presence of ascorbate. Note the parallel alignment and ordered distribution of the control cells that display a clear spindle-like shape. On the other hand, all HFS fibroblasts display bizarre shapes and are irregularly arranged on the growing surface. Bar = 500 µm. (**d**) *ANTXR2*, *p21* and *LMNB1* expression levels were assessed by RT-qPCR in the indicated fibroblasts. Of note, *ANTXR2* expression by HFS #1 fibroblasts is comparable with control levels, but protein levels are strongly reduced in these fibroblasts, as previously shown in (1). Three independent samples, ordinary 1-way ANOVA tests were used (HFS #1 and #2 vs CTRL #1 and #2, HFS #3 and #4 vs CTRL #3 and #4. (**e**) The graphs show the relative percentage of different nuclear lamina defects in control and HFS fibroblasts. n = 2, 100 cells per sample. (**f**) Quantification of nuclei with an abnormal morphology in the indicated fibroblasts plated for 24 hours on the indicated substrates. n = 3. Each data point is an independent sample, 100 cells per sample, with 2-way ANOVA. (**g**) Control and HFS fibroblasts were allowed to spread on glass coverslips coated with collagen I or fibronectin. Cells were fixed at the indicated time intervals and labeled with phalloidin. The graphs show the quantification of cell area on the different substrates. n = 3. A total of 10–22 cells were measured for each condition and each time point. Ctrl, control; HFS, hyaline fibromatosis syndrome.

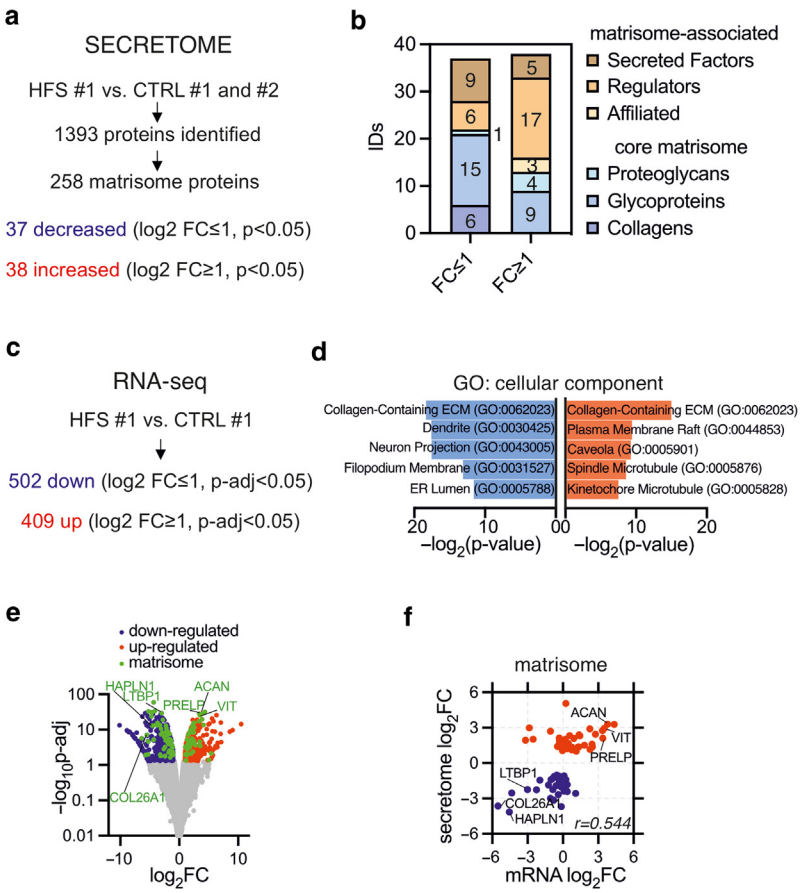

Supplementary Figure S2. Integrated secretome and transcriptome analysis reveals dysregulation of matrisome components in HFS fibroblasts. (**a**) Schematic overview of the experimental workflow for the secretome analysis. Fibroblasts from 2 controls and 1 patient with HFS were kept in serum-free medium supplied with ascorbate for 72 hours. The culture media were collected, digested, and subjected to label-free quantitative mass spectrometric analysis. Triplicates were analyzed for each control line and duplicates for the HFS cells. (**b**) Stacked bar chart showing the distribution within the matrisome subgroups of significantly decreased and increased proteins (fold change ≤ -1 or ≥ 1 respectively, $P < .05$) in the culture medium of HFS fibroblasts when compared with both control lines. (**c**) Schematic diagram of the transcriptomic analysis in HFS #1 versus CTRL #1 fibroblasts. n = 3 for each cell line. Total RNA extraction was extracted with TRIzol (Invitrogen). RNA sequencing was performed by Novogene Europe using 150-bp paired-end sequencing on an Illumina platform. After cDNA library construction, sequencing, and filtering, reads were mapped to the Mus musculus reference genome (GRCm38/mm10) using Hisat2, version 2.0.5. Read numbers mapping to each gene were obtained using FeatureCounts (version 1.5.0-p3) and converted to FPKM. Differential gene expression analysis was done using DESeq2 in R. (**d**) Gene ontology analysis (https://maayanlab.cloud/Enrichr/) of downregulated (blue bars) and upregulated (red bars) genes (fold change ≤ -1 or ≥ 1, respectively, adjusted $P < .05$) in HFS #1 versus CTRL #1 fibroblasts. (**e**) Volcano plot visualizing the transcriptomic data. Significantly downregulated and upregulated genes are shown in blue and red, respectively. Differentially expressed matrisome genes are highlighted in green. (**f**) Scatterplot with associated correlation coefficient of matrisome components that were found to be significantly decreased or increased in the secretome of HFS patient fibroblasts #1 vs CTRL #1. The fold change at the protein level is displayed on the X-axis and the corresponding fold change of the transcript on the Y-axis. FC, fold change; FPKM, fragments per kilobase of transcript per million mapped reads; GO, gene ontology; HFS, hyaline fibromatosis syndrome; ID, identification; p-adj, adjusted *P*-value.

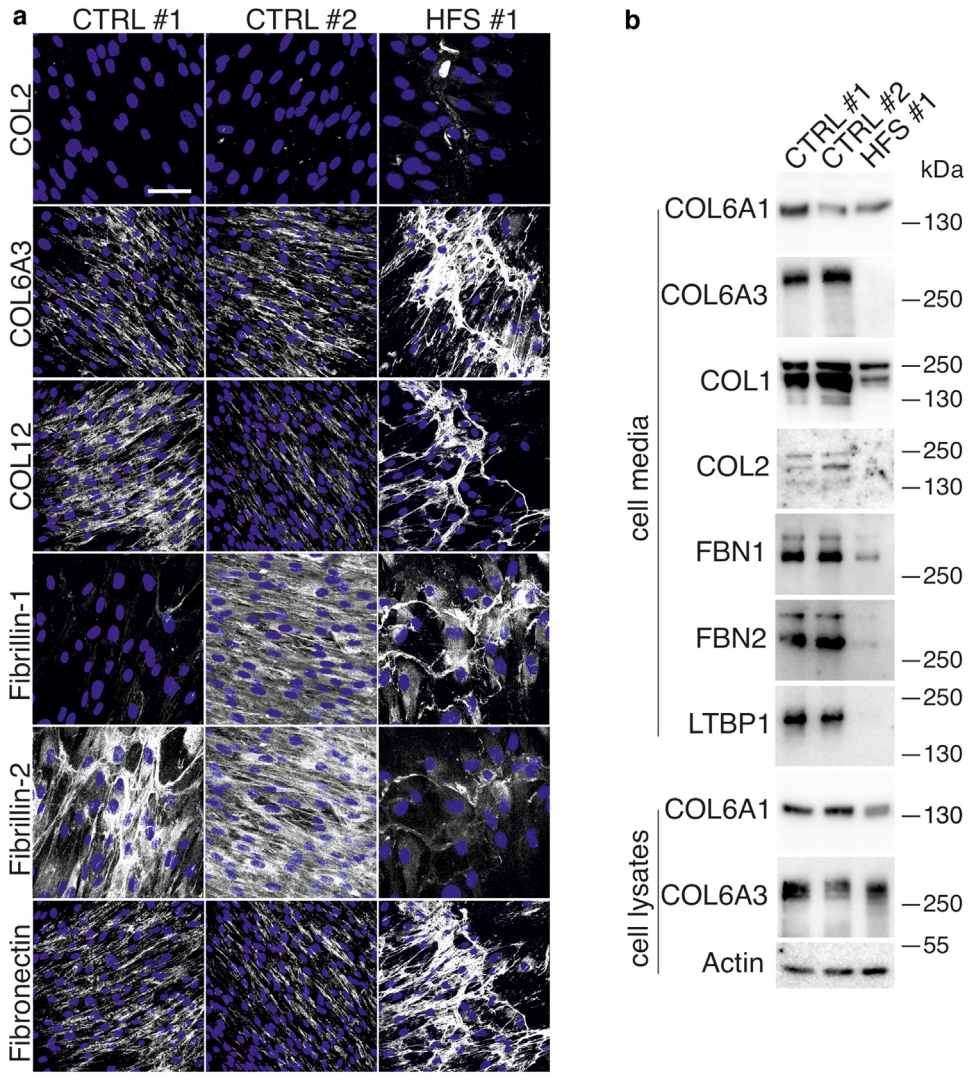

Supplementary Figure S3. Altered extracellular matrix composition and organization in HFS fibroblasts. (**a**) ECM of control and HFS fibroblasts was labeled with the indicated antibodies revealing both qualitative and quantitative differences in comparison with those of the control cells. The different architecture of the fibrils was consistent for all the proteins that showed a fibrillar deposition. Note the presence of small collagen II aggregates only in the patient monolayer, in line with the presence of other cartilage-specific ECM components and a "chondroid" phenotype of the patient fibroblasts. Bar = 100 μm. (**b**) Serum-free conditioned media and cell lysates from the indicated fibroblast lines were analyzed by immunoblotting using the indicated antibodies. The analysis showed a general reduction in the levels of core-matrisome components in agreement with the proteomic data. ECM, extracellular matrix; HFS, hyaline fibromatosis syndrome.

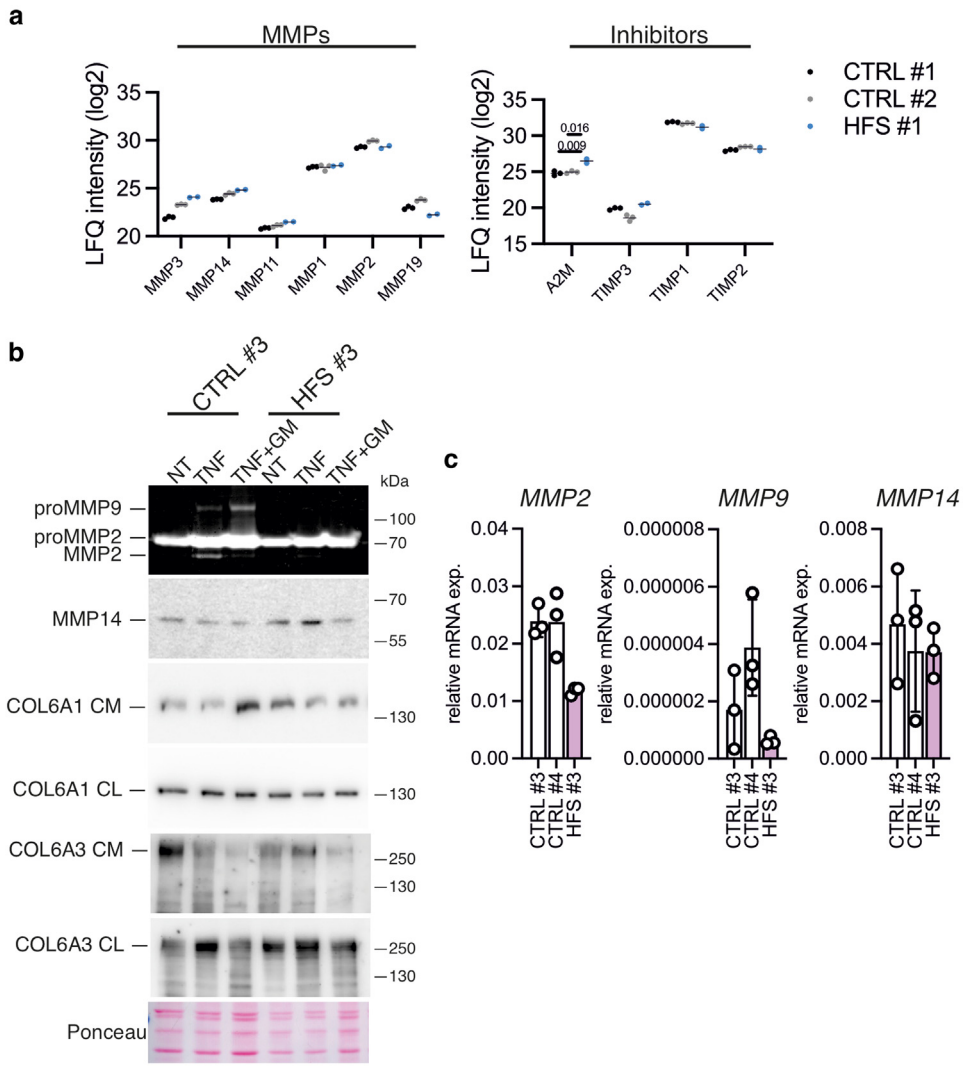

Supplementary Figure S4. Dysregulated MMP activity and expression in HFS fibroblasts. (**a**) Dot plots showing the abundance of secreted MMPs and MMP inhibitors in the culture medium of the indicated fibroblasts as assessed by label-free quantitative mass spectrometry. n = 3 (CTRL #1 and 2) and n = 2 (HFS #1). Only A2M showed values that were significantly different in HFS cells compared with those in the 2 controls. (**b**) Gelatin zymography and western blot of supernatants and cell lysates derived from the indicated fibroblast lines. Cells were left untreated (denoted as NT) or treated with 10 ng/ml TNFα alone or with 50 μM of the MMP inhibitor GM6001 for 48 hours before medium collection and analysis. Ponceau staining was used as a loading control. (**c**) RT-qPCR analysis of *MMP2*, *MMP9*, and *MMP14* expression in the indicated fibroblasts. n = 3 independent samples, with unpaired *t*-test. A2M, α2-macroglbulin; CTRL, control; HFS, hyaline fibromatosis syndrome; MMP, matrix metalloproteinase.

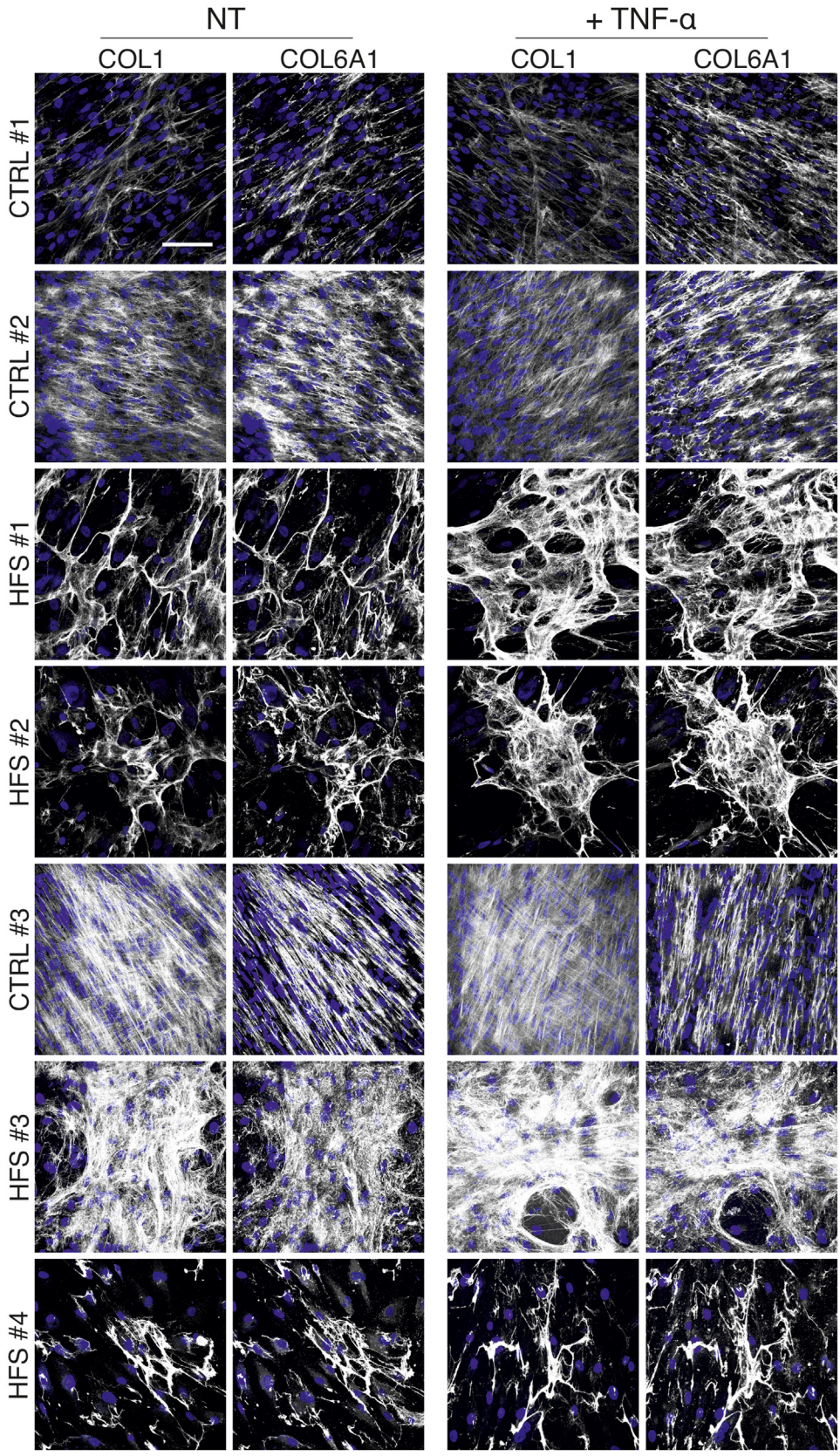

Supplementary Figure S5. Disrupted collagen fibrillogenesis in HFS fibroblasts is unaffected by TNF-α treatment. Control and HFS patient fibroblasts were cultured for 7 days in the presence of ascorbate, with or without supplementation with 10 ng/ml TNF-α. Cell monolayers were then fixed and stained for collagens I and VI. All HFS fibroblast lines showed grossly disrupted fibril formation for both collagens, and this pattern was not significantly altered by TNFα treatment. TNFα also did not affect the thin, oriented collagen fibrils produced by control fibroblasts. NT denotes not treated. Bar = 100 μm. HFS, hyaline fibromatosis syndrome.

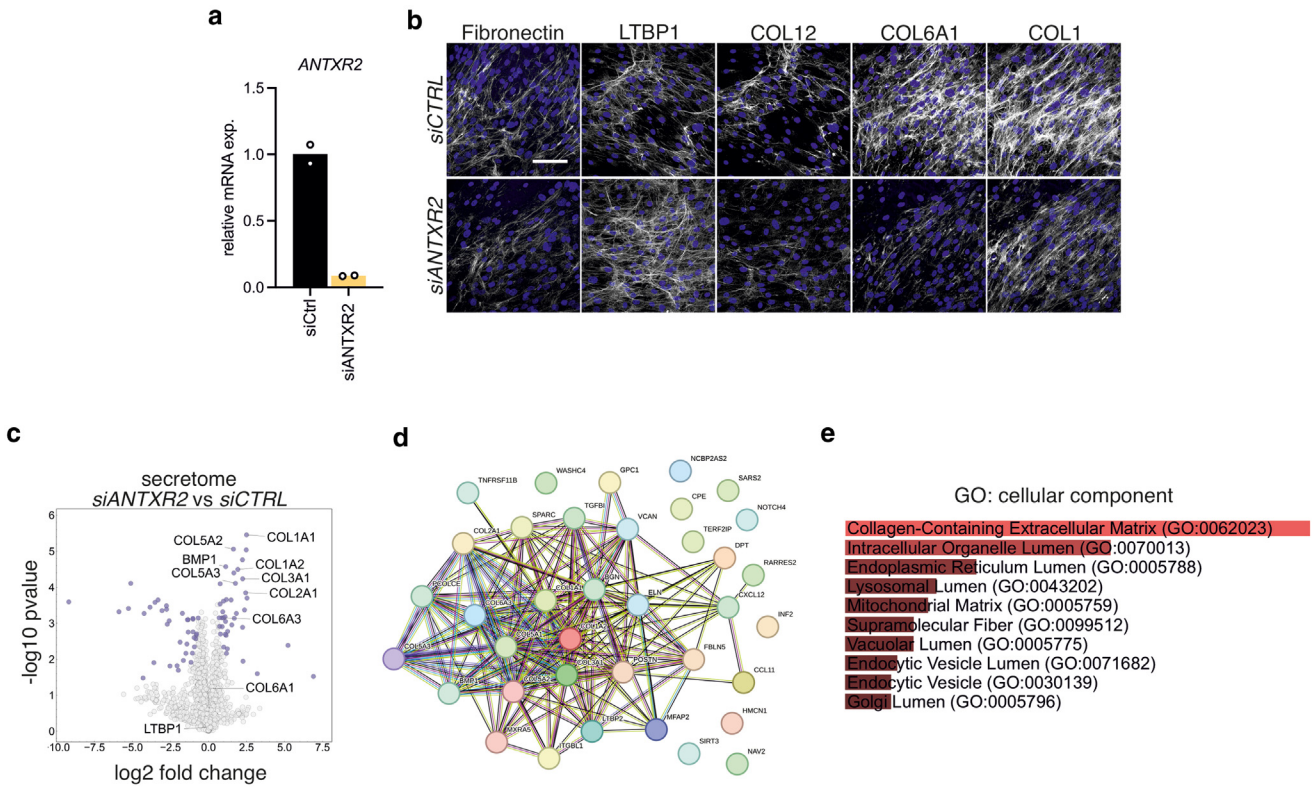

Supplementary Figure S6. Secretome profiling of ANTXR2-depleted fibroblasts reveals ECM-associated changes independent of fibril structure. (**a**) Validation of *ANTXR2* knockdown in primary human dermal fibroblasts by RT-qPCR analysis. (**b**) Fibroblasts transfected with a siCTRL or a combination of 2 siRNAs targeting ANTXR2 (siANTXR2) were cultured for 5 days, fixed, and stained with antibodies against the indicated ECM components. No significant differences in fibril quality were observed between the 2 groups. (**c**) Volcano plot of secretome analysis of fibroblasts transfected as in **a** and **b**. Significantly dysregulated proteins are highlighted in purple, and selected ECM proteins are labeled. (**d, e**) STRING network and GO enrichment analysis (https://maayanlab.cloud/Enrichr/) of the 40 proteins found to be significantly increased in the secretome of ANTXR2-depleted fibroblasts. ECM, extracellular matrix; GO, gene ontology; siANTXR2, ANTXR2-targeted small interfering RNA; siCTRL, control-targeted small interfering RNA; siRNA, small interfering RNA.

Supplementary Table S1. Clinical and Genetic Data of Primary Cell Lines

Fibroblast Line	Sex	Age	ANTXR2 cDNA NM_058172.6	ANTXR2 Protein NP_477520.2
CTRL #1	F	3 years	WT	WT
CTRL #2	M	7 months	WT	WT
CTRL #3	F	14 years	WT	WT
CTRL #4	M	15 years	WT	WT
HFS #1[1]	F	4 years	c.[116G>T];[1074del]	p.[(Cys39Phe)];[(Ala359His*fs**50)]
HFS #2[1]	M	6 months	c.[945T>G];[945T>G]	p.[(Cys315Trp);[(Cys315Trp)]
HFS #3	M	16 years	c.[1180_1428del];[1180_1428del]	p.[(Val394_Glu476del)];[(Val394_Glu476del)]
HFS #4	F	14 years	c.[1180_1428del];[1180_1428del]	p.[(Val394_Glu476del)];[(Val394_Glu476del)]

Abbreviations: F, female; HFS, hyaline fibromatosis syndrome; M, male; WT, wild type.
[1]Already described in Deuquet et al (2011) as patients 1 and 3, respectively.

Supplementary Table S2. Clinical Characteristics of the Patients Included in this Study

Clinical and Molecular Features	Patient HFS #1	Patient HFS #2	Patient HFS #3	Patient HFS #4
Sex	F	M	M	F
Papular skin lesions	+	+	+	+
Thickened skin	−	+	+	−
Gingival hyperplasia	−	+	+	+
Perianal nodules	+	+	+	+
Large nodules/tumors	−	−	+	+
Hyperpigmented plaques	−	−	+	+
Joint contractures	+	+	+	+
Osteoporosis/osteopenia	−	−	+	+
Osteolysis	−	−	+	+
Persistent diarrhea	+	−	+	+
Recurrent SIRS	−	−	−	−
Visceral involvement	−	+	+	+
Short stature	−	+	+	−
Failure to thrive	−	−	+	(+)

Abbreviations: F, female; HFS, hyaline fibromatosis syndrome; M, male; SIRS, systemic inflammatory response syndrome.